Emissive cathode immersed in a plasma: plasma-cathode interactions, operation and stability - Supplementary material

F Pagaud[1], V Dolique[1], N Claire[2] and N Plihon[1]

[1] ENSL, CNRS, Laboratoire de physique, F-69342 Lyon, France

[2]Aix Marseille Univ, CNRS, PIIM, Marseille, France

Submitted to: *Plasma Sources Sci. Technol.*

A. Transmittance of the glass window

The glass window separating the cathode and the pyrometer absorbs partially the light at 650 nm. Its transmittance has been quantified from relative measurements following the following protocol:

1. The cathode is put under vacuum in front of an unspecified borosilicate window and heated at a fixed heating current I_h. Its apparent temperature T_W is measured at an apparent given emissivity ϵ_a, arbitrarily set for the pyrometer (which takes into account the real emissivity of the cathode and the transmittance of the unspecified window).
2. Then the borosilicate window used for the experiment presented in section 3 is added outside of the vacuum chamber between the pyrometer and the cathode. The emissivity paramater of the pyrometer r is adjusted to ϵ' in order to recover a measured temperature equal to T_W, obtained at step 1. This relative measurement provides the transmittance τ_g of the borosilicate window as the ratio ϵ'/ϵ_a.
3. The experiment is repeated for various values of I_h and ϵ_a to ensure reproducibility.

The real emissivity ϵ used in the experiment in section 3 is then $\epsilon = \epsilon_W \tau_g$, with ϵ_W the tungsten emissivity. The correction factor τ_g is displayed in figure A for two different initial values of ϵ_a as a function of I_h. Dark blue (respectively light orange) solid lines represent the mean values of the dark circle (resp. light square) markers, pale areas represent the standard deviation for each dataset. The final value of the glass transmittance has been assessed at 80 ±4 %.

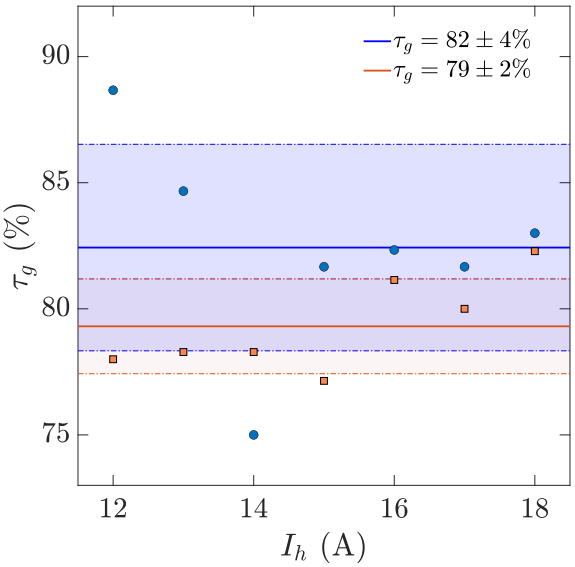

Figure A: Transmittance of the glass window between the pyrometer and the cathode for $\lambda = 650$ nm for two different scans in I_h.

B. Videos of operation, measurements and simulation

`Video_1.mp4` shows the effect of thermionic emission on the plasma column. It is a side view of the inside of the plasma chamber at 1 mTorr, 170 G and 1 kW. A drawing of the setup is found at the beginning: the RF source is at the left end, while the cathode faces the plasma at the other end of the chamber. First the plasma is ignited using the RF source on the left side, resulting in a 10-cm wide plasma column while the cathode is hot and floating. Then the cathode is negatively biased and emits primary electrons from the right end, creating a denser 2-cm wide plasma core. The strong emission at the cathode is sustained for a few seconds, and finally the power of the RF source is shut down.

`Video_2.mp4` is a recording of the light intensity through the pyrometer for the experimental conditions presented in section 3. The cathode is observed through the pyrometer, which filters the light at 650 nm. Initially, the reference gray body of the pyrometer (Λ shape) is brighter than the cathode. The plasma is first ignited and the cathode is negatively biased, resulting in a strong thermionic emission and a progressive cathode heating, finally ending in a divergent regime. The heterogeneous intensity profile is highlighted here. An homogeneous profile is quickly recovered once the plasma is turned off.

`Video_3.mp4` shows simultaneously the raw pyrometer measurements (left panel), the temperature profile along the cathode extracted from the raw pyrometer measurements (central panel) and the emitted current (right panel).

`Video_4.mp4` shows the temporal evolution of the measured temperature profile and the numerical resolution for $I_h = 16.2$ A, $V_b = -62$ V and $\beta = 1.01$.

`Video_5.mp4` shows the temporal evolution of

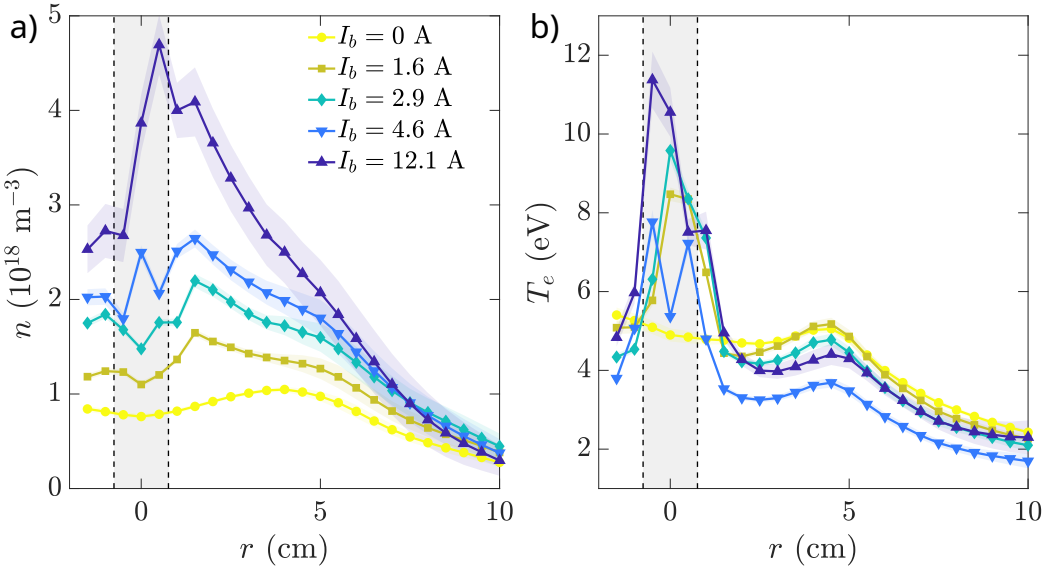

Figure B: Radial evolution of *a)* the plasma density and *b)* the electron temperature for various currents I_b. The gray areas represent the location of the cathode.

the spatial profiles of the heating and cooling terms (powers per unit length) for the numerical solution. The red positive terms are the source terms while the blue negative terms are the sink terms. Conduction is not represented here but represents only a significant part at the 15-mm extremities. The black dashed-line is the sum of all the terms, conduction included.

C. Plasma density increase with thermionic emission

The plasma density increases with the cathode current I_b. The evolution of the plasma density with the emitted current is taken into account in Section 4 for the computation of the contribution of the ion saturation current in the total cathode current. It is also taken into account in Section 5 for the thermal modeling, including the power deposition from the emissive cathode.

The radial evolution of the plasma density and the electron temperature are shown in figure B for $V_b = -60$ V for various values of the total cathode current I_b.

The power supplied by the cathode to the plasma contributes to ionization and heating in addition to the RF antenna, resulting in a broad increase in density at the plasma core, and a localized increase of the electron temperature at the core. The variations of the plasma density n as a function of I_b are shown in figure C for two different biases of the cathode): $V_b = -60$ V (circles) for $V_b = -40$ V (squares). The influence of the increase of electron temperature on the ion saturation current is also assessed in figure C for $V_b = -60$ V, where $n\sqrt{T_e}/\sqrt{T_{e,0}}$ is shown as full diamond, with $T_{e,0} = 4.5$ eV the temperature at $I_b = 0$.

Let us first discuss the evolution of the plasma density taken into account for the estimate of the ion saturation current in Section 4, assuming that the electron temperature remains constant at $T_{e,0} = 4.5$ eV. The linear evolution considered in Section 4 is shown as a dashed red line ($n = 10^{18} + 3 \times 10^{17} I_{em}$). This estimated density increase slightly overestimates the density increase (nearly 20 %) and slightly underestimates the real ion saturation current (nearly 20 %). Since the contribution of the ion saturation current on the total cathode current is minor in regards with thermionic emission, we consider that our linear modeling is accurate enough for the computation of the ion saturation current with I_b as computed in Section 4.

Let us now discuss further the power balance used in the model of Section 5. When the cathode is left floating or cold (i.e. $I_b = 0$), the plasma density n_0 is sustained by the RF antenna alone and is assumed to be homogeneous in a cylinder of radius $R = 5$ cm. The density increase due to the cathode is assumed to be linear from the edge of the plasma (5 cm) to the core (0 cm) accordingly to the experimental measurements (see figure B) and the plasma density is modelled as $n(r) = n_0 + \Delta n \left(1 - \frac{r}{R}\right)$. T_e is assumed to be independent of the cathode current and cathode bias voltage. The global model assumes that the total absorbed power (i.e. the radio-frequency power and the cathode power) is balanced by the power losses at the walls, *i.e.* the recombination of each electron-ion pair releases $\mathcal{E}_\mathrm{T} = 75$ eV [1, 2].

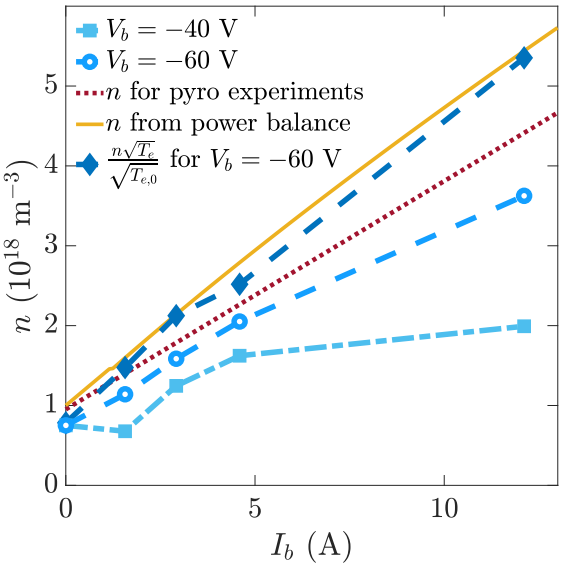

Figure C: Density at the plasma core as a function of current through the cathode I_b for two values of V_b. The empirical and numerical values used to compute I_{is} at $T_{e,0} = 4.5$ eV are shown respectively in dotted and solid lines. The density corrected by the experimental electron temperature for $V_b =$ –60 V is also displayed.

The power input from the cathode to the plasma is provided by thermionic electrons as:

$$P_{cath} = \int_0^{l_W} I_{em}(x)(\Phi_p - V_c(x))\ \mathrm{d}x \tag{1}$$

On the other hand, the increase in losses δP_{losses} is associated to the density increase $\Delta n\left(1 - \frac{r}{R}\right)$ as

$$\delta P_{losses} = \Delta n \frac{\pi R^2}{3} \sqrt{eT_e/m_i} e\mathcal{E}_\mathrm{T} \tag{2}$$

Assuming stationarity, one can compute the density at the core ($r = 0$ cm) as:

$$n = n_0 + \frac{3P_{cath}}{\pi R^2 \sqrt{eT_e/m_i} e\mathcal{E}_\mathrm{T}} \tag{3}$$

which is shown as a full yellow line in figure C and reproduces well the experimental data corrected in T_e.

D. Technical details on the numerical simulation

The numerical simulation solves an integro-differential heat equation. The time step is 10^{-3} s and the spatial step is 10^{-3} m. This resolution verifies the Courant-Friedrich-Levy condition for the heat equation

$$\frac{\lambda_W}{\rho C_p} \frac{\mathrm{d}t}{\mathrm{d}x^2} \sim 2.5 \times 10^{-2} \leq 1 \tag{4}$$

For the computation of iteration N, the integral term is computed manually from the temperatures at N-1. The equation is solved numerically using the function `pdesolver` from MATLAB. The initial temperature profile of the cathode is obtained from an initially homogeneous profile, then freely evolving in absence of plasma for 5 seconds.

E. Temperature dependence of tungsten thermophysical properties

The temperature-dependent thermophysical properties for tungsten are displayed in figure D: thermal conductivity λ_W [3, 4], electrical resistivity ρ_W [3, 4], specific heat C_p [3, 4] and hemispherical total emissivity ϵ_{eff} [5] from top left to bottom right. The first three quantities are fits based on experimental data in the range [1800 K; 3200 K] while the last one is the best fit according to the works of Matsumoto *et al.* [5] in the range [2000 K; 3400 K].

F. Setting the value of the α parameter

The temperature of the cathode in absence of plasma has been measured experimentally and compared to numerical results. The parameter α accounts for heating of the neighboring turns of the filament through radiation as explained in Figure 6. The evolution of the (homogeneous) temperature T_W as a function of I_h is shown in figure E. The value of the parameter α is inferred from the best agreement between the experimental values and the numerical solution of the model described in Section 5. The case $\alpha = 0$ (black dotted line) underestimates T_W by 50 K to 75 K ($\sim$ 2.5 % in relative value). A very good agreement is observed for $\alpha = 0.15$ (black dashed line), over the whole range of I_h. This latter value was retained for all numerical simulations.

G. Influence of λ_{Cu} in the boundary conditions

The conductivity of copper is involved in the boundary conditions as described in section 5.1.2. Its value is corrected because of the poor thermal contacts between the copper rods that are used to clamp the cathode and the tungsten filament. Its influence on the temperature profile along the cathode is shown in figure F(a) and the consequences on I_b is displayed in figure F(b) for λ_{Cu} in the range [20 W/(m K) ; 80 W/(m K)]. The blue area represents the spans of T_W and I_b for higher values of λ_{Cu} up to 80 W/(m K) while the red one represents T_W and I_b for lower λ_{Cu} down to 20 W/(m K).

One can see that the initial temperature profile along the cathode is not modified except at the 15-mm

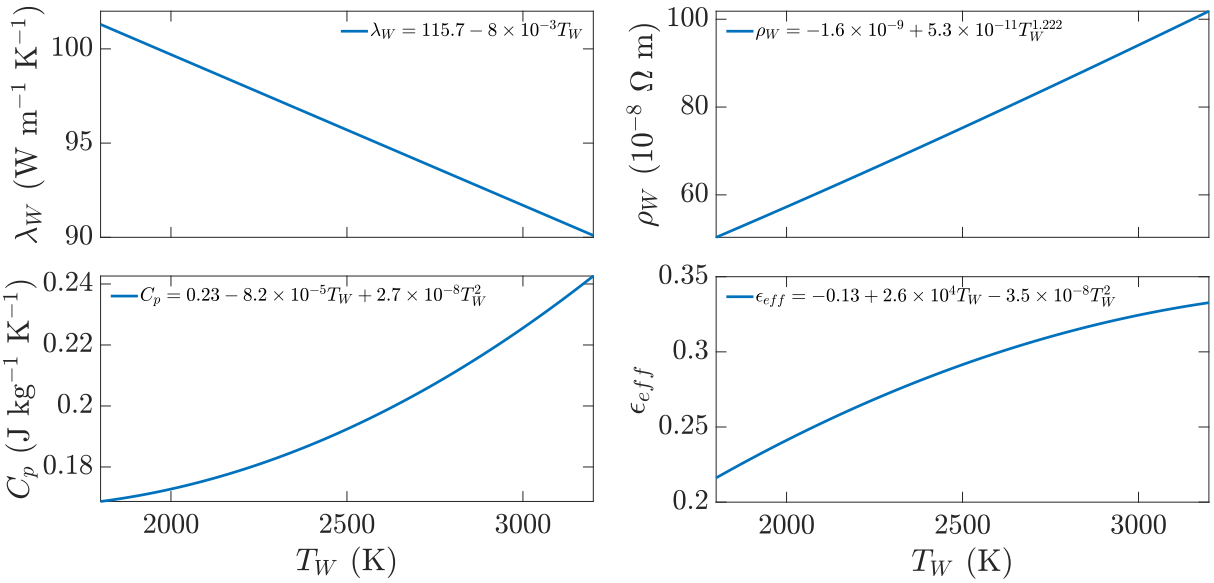

Figure D: Thermophysical properties of tungsten as a function of temperature.

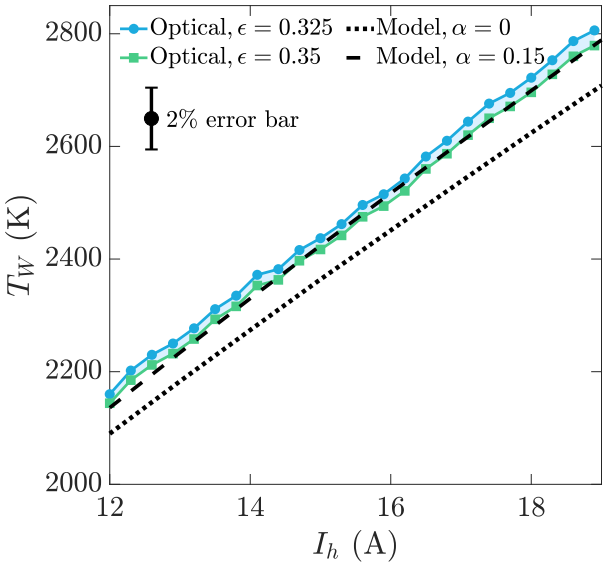

Figure E: Comparison of optical measurements (solid lines) and numerical results (black lines) of T_W for different values of I_h in absence of plasma. Numerical values of T_W are displayed with $\alpha = 0$ (dotted line) and $\alpha = 0.15$ (dashed line). The error bar represents the margin of error for optical measurements.

extremities, where a significant difference is observed. It results in similar I_b trends which differ progressively because of the small variations in initial conditions and the different losses at the boundaries. Yet this effect remains minor, as the trends in T_W and I_b are still similar despite spanning a wide range of λ_{Cu}.

H. Φ_p dependency on I_b

Measurements of Φ_p at the core of the plasma with an emissive probe as a function of I_b are shown in figure G for three different experiments (blue solid lines). Besides the technical challenges of using emissive probes in a non-stationary plasma, the dependence of Φ_p on I_b is not fully understood yet. Its variations are thus implemented empirically in the numerical simulation. The best power law fit used for the simulations is presented here as the black dotted line.

I. Influence of β

The most sensitive numerical parameter of the full numerical model is β, introduced in section 5.1.1. Its influence is illustrated in figure H as one can see temperature profiles obtained for β values ranging from 0.5 to 0.98. The insert shows the temporal evolution of I_b for three values of β. One clearly sees the influence of β on the temporal evolution of the cathode current. the best agreement with the experimental data is observed for $\beta = 1.01$.

J. Source code

A github repository containing the source codes for the simulation is available here: `https://github.com/FrancisPagaud/Emissive-Cathode-Model.git`

References

[1] Lieberman M and Lichtenberg A 2005 *Principles of Plasma Discharges and Materials Processing* (John

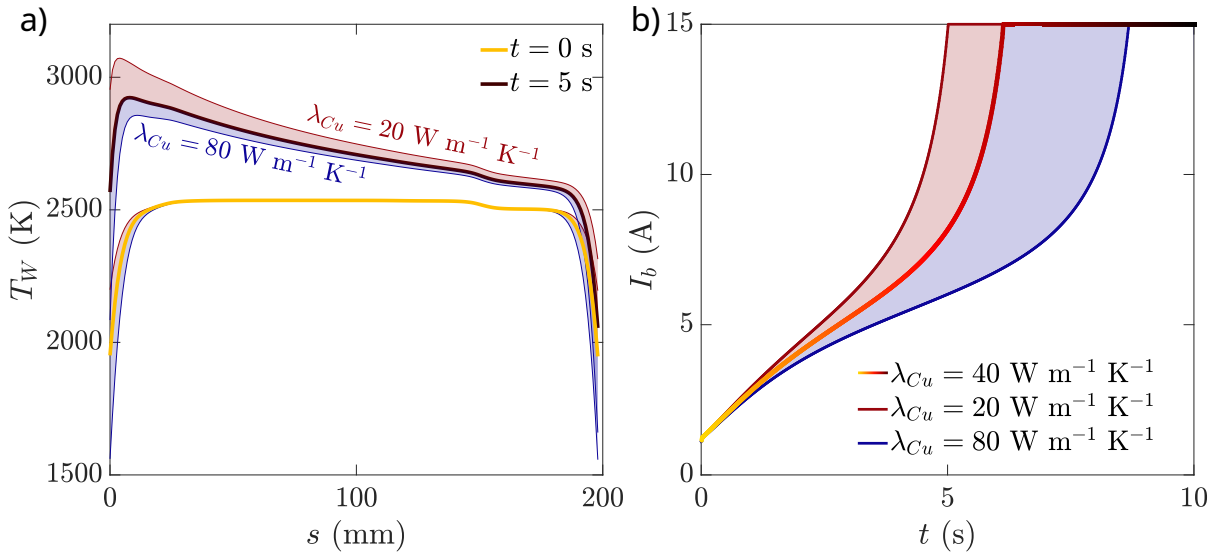

Figure F: *a)* Temperature profile along the cathode ; *b)* Currents I_b for 3 different values of λ_{Cu}.

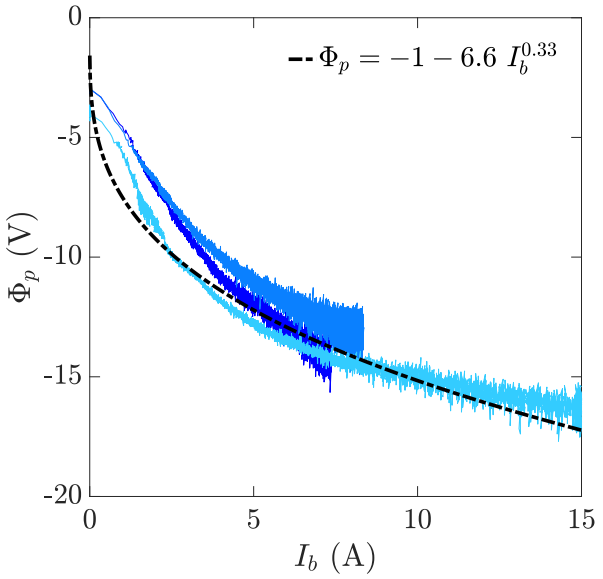

Figure G: Φ_p measurements as a function of I_b. The black dotted line represents the best power law fit for the light blue curve.

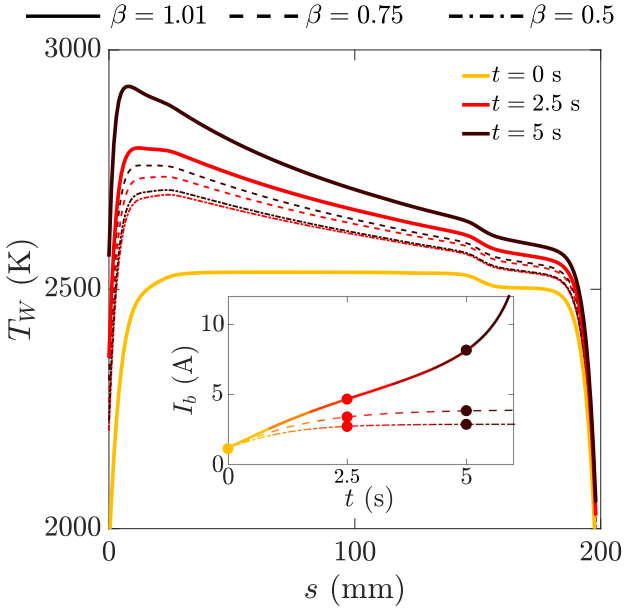

Figure H: Temperature profiles of the cathode at $I_h = 16.2$ A and $V_b = -60$ V for $\beta = 0.5$ (dotted lines), $\beta = 0.75$ (dashed lines) and $\beta = 1.01$ (solid lines). Insert: I_b over time for the three cases.

Wiley & Sons, Ltd)

[2] Chabert P and Braithwaite N 2011 *Physics of Radio-Frequency Plasmas* (Cambridge University Press)

[3] White G K and Minges M L 1997 *Int J Thermophys* **18** 1269–1327

[4] Desai P D, Chu T K, James H M and Ho C Y 1984 *Journal of Physical and Chemical Reference Data* **13** 1069–1096

[5] Matsumoto T, Cezairliyan A and Basak D 1999 *International Journal of Thermophysics* **20** 943–952